Toward a Nonlinear Identification of the Atmospheric Response to ENSO

A. HANNACHI

Atmospheric Physics, Clarendon Laboratory, Oxford, United Kingdom

(Manuscript received 14 December 1999, in final form 26 September 2000)

ABSTRACT

Motivated by the need to understand the nature of the remote atmospheric climate signal associated with El Niño–Southern Oscillation (ENSO), the question is addressed of estimating the nonlinear atmospheric response to ENSO using state-of-the-art general circulation models (GCMs). A set of multidecadal integrations of the Hadley Centre GCM model, HadAM1, is considered and the focus is on the variability of the winter 500-mb heights over the North Pacific and North Atlantic basins. The method is based on optimally filtering the signal out given an estimate of the covariance matrices of the ensemble mean and the internal noise, respectively, and requires that the ensemble mean be split into clusters according to the phase of the Southern Oscillation and then the signal in each cluster found. Over the North Pacific, La Niña appears to trigger the negative Pacific–North American (PNA) oscillation while during El Niño the response is degenerate, that is, with more than one response pattern, where the first one has a zonally stretched PNA-like structure with a north–south seesaw signature and the second one is similar to the tropical Northern Hemisphere pattern. None of them is precisely the reverse of the response corresponding to La Niña (−PNA). A similar behavior is observed over the North Atlantic where a tripole pattern emerges during La Niña, whereas the first pattern obtained during El Niño shows a (tilted) dipole structure with a north–south seesaw.

1. Introduction

Despite the many ENSO-related investigations that have been carried out, the nature of the atmospheric climate signal associated with ENSO is still an ongoing debate within the climate community, particularly the nature of the remote signal. Although several analyses have shown, at least qualitatively, that the extratropical (and also tropical) atmospheric response to tropical forcing is essentially a linearly controlled phenomenon (Hoskins and Karoly 1981; Horel and Wallace 1981), there is a general consensus to believe that this response is basically nonlinear.

In the first paradigm, the atmospheric response associated with ENSO is linear whereby the signal anomalies during El Niño and La Niña, respectively, are reverse of each other. However and as pointed out by Hoerling at al. (1997, hereafter HKZ97) this paradigm, which emerges primarily from linear analyses, cannot be fully supported because of the nonlinear nature of the thermodynamic control on deep convection. HKZ97 argued that the global atmospheric response to tropical SST forcing is inherently nonlinear. They found using observations as well as model simulations that the atmospheric response to extreme phases of tropical SST anomalies exhibit appreciable nonlinearity in agreement with other previous studies (e.g., Livezey et al. 1997). The nonlinearity observed in HKZ97 is between SST and atmospheric forcing in the Tropics and also between atmospheric forcing and extratropical response. It is therefore important to have an estimate of this nonlinear response and this paper attempts to provide the first steps in this direction.

In this study the question is addressed of quasi-linearity and nonlinearity in the atmospheric response to ENSO based on a nonlinear algorithm to detect signals from noise-contaminated data given an estimate of the noise covariance and using an ensemble of multidecadal simulations of the Hadley Centre atmospheric GCM model. The manuscript is organized as follows. Section 2 presents the model variability. In section 3 I briefly outline the approach. The application to the winter 500-mb geopotential heights over the North Pacific and the North Atlantic basins are presented in section 4. A summary and conclusions follow in the last section.

2. Internal and ensemble mean variability in the model

The model focused on in this study is the Hadley Centre model, HadAM1, of the U.K. Met. Office. It is a gridpoint model with resolution 2.5° lat × 3.75° long and 19 hybrid vertical levels. It has a gravity wave drag

Corresponding author address: Dr. A. Hannachi, Department of Meteorology, University of Reading, 2 Earley Gate, P.O. Box 243, Reading RG6 6BB, United Kingdom.
E-mail: han@met.reading.ac.uk

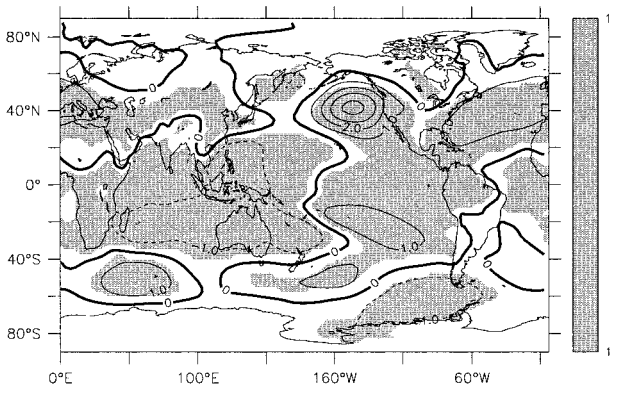

FIG. 1. DJF SLP anomalies composite during cold (La Niña) events. Contour interval 1 mb. Positive (negative) anomalies are shown by solid (dashed) contours. Shaded areas indicate the 95% confidence level.

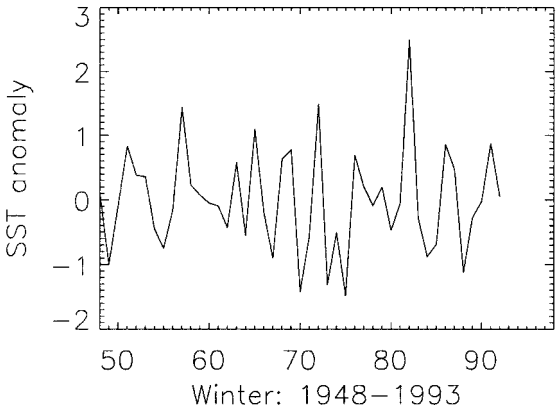

FIG. 2. The ENSO index estimated by averaging the DJF SST anomalies over the Niño-3 region (5°S–5°N, 150°–90°W) (°C).

and radiation schemes with radiative fluxes computed in four longwave and six shortwave bands, a penetrative convection scheme, and a land surface scheme (see Davies et al. 1997; Phillips 1994 for more details). The model integrations consist of six members integrated from October 1948 to December 1993 forced with observed global sea-ice and sea surface temperature (Parker et al. 1995). Renshaw et al. (1998, hereafter RRF98) used the same integrations to study the impact of ENSO on the low-frequency variability in the North Pacific–American sector while Venzke et al. (1999, hereafter V99) focused on the mean sea level pressure (MSLP) to study the response to the Atlantic SST. It has been shown (RRF98) that the model responds reasonably well to ENSO throughout the globe with interannual variations of the Southern Oscillation index being particularly well captured. Figure 1, which is similar to Fig. 2 of RRF98 except that their winter is based on January–March, indicates composites of (DJF) MSLP anomalies during cold (La Niña) events along with the 95% confidence level. The composite over the warm events (not shown) is the reverse of Fig. 1. Here warm and cold events are defined by the sign of the Niño-3 index. Note in particular the significant influence of ENSO in the (model) North Atlantic.

The monthly anomaly fields of the 500-mb height are obtained by subtracting the monthly climatology, or grand mean, from the monthly data of the ensemble members. The grand mean is defined as the time mean of the ensemble average and the ensemble mean as the time series of the 45 seasonal (winter) means derived by averaging the six members of the ensemble. Here the winter season is defined as December–February (DJF) and the corresponding winter fields are obtained by averaging DJF anomalies. Two geographical areas of interest are considered in this study; the North Pacific (2.5°–75°N, 123.5°E–60°W) and the North Atlantic (2.5°–72.5°N, 90°W–0°). This area separation is important mostly because the Pacific region provides an ideal test bed to study the atmospheric response to ENSO (RRF98; HKZ97). Because we are mainly interested in the influence of external, primarily tropical (Pacific) SST, forcing on atmospheric variability and since the focus here is on ENSO we choose for the latter the Niño-3 index (Fig. 2) obtained by averaging the DJF SST anomaly over the Niño-3 region (5°S–5°N, 150°–90°W).

a. Internal variability estimates

The noise fields are estimated by subtracting the ensemble mean from each ensemble member. The combined fields thus obtained provide a good estimate of the internal noise because of the relatively long record obtained from independent realizations.

1) NORTH PACIFIC SECTOR

The first two EOFs are displayed in Fig. 3. They explain respectively 28% and 20% of the total variability. The first one indicates a north–south seesaw reminiscent of the North Pacific oscillation (NPO). The second mode emerges as the familiar Pacific–North American (PNA) teleconnection pattern (Wallace and Gutzler 1981). Table 1 displays the variances explained by the different modes of variability over different geographical locations along with their standard errors as estimated from the rule of thumb of North et al. (1982) and where we assume one degree of freedom for each season.

2) NORTH ATLANTIC SECTOR

Figure 4 displays the leading two EOFs. The first one with 37.5% variance (Table 1) comes out as the familiar North Atlantic oscillation (NAO) a north–south seesaw with respective centers over the central North Atlantic and Greenland. The second mode with 21% variance shows a tilted southeast–northwest dipole. The southern center is weaker than the northern one. The third mode (not shown) has a zonally oriented structure with centers

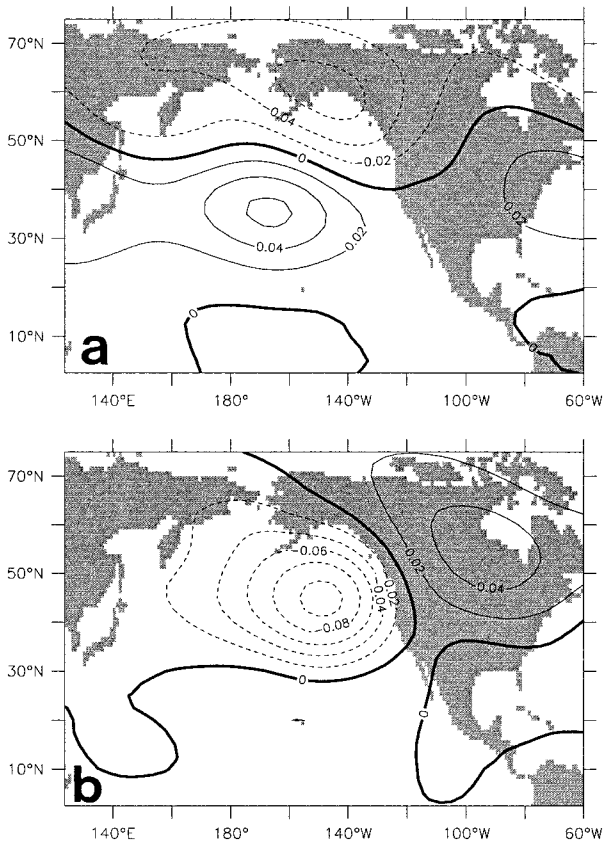

FIG. 3. (a) The first and (b) the second North Pacific EOFs of the internal variability of the winter geopotential height at 500 mb. Contour interval arbitrary. Positive (negative) contours are solid (dashed).

over eastern Canada, south of Iceland, and the western Mediterranean. To verify that the internal variability is independent of the ENSO, the effect of this latter was removed by regression onto the ENSO index. Noise fields and corresponding EOFs are then computed as before, and the modes of variability are found to be similar to those computed previously and with almost the same corresponding explained variances.

b. Modes of variability of the ensemble mean

The leading mode of variability of the ensemble mean can generally provide a first approximation of the model response to varying SST boundary conditions. A priori there is no reason to believe that this mode should necessarily coincide with the corresponding mode of the internal noise especially when the signal-to-noise (S:N) ratio is large as in the North Pacific (Rowell 1998) or also over the North Atlantic (Rowell 1998; V99). In a linear paradigm it is certainly true that the biggest response to forcing is in free modes of variability and that in fact the order of the response and internal modes could simply be swapped. However, in the presence of nonlinearity the response could be somewhat different from the internal modes and this is the issue we would like to address. Note that here we are rather interested in objectively comparing both modes of variability without any prior judgment on the (dis)similarity between forced and free variability.

TABLE 1. Explained variance (%) of the first four EOFs of the internal variability, the full and ENSO-regressed ensemble mean of the winter 500-mb height over the North Pacific and North Atlantic sectors. Sampling errors are also displayed.

	EOF rank	Internal variability	Ensemble mean	ENSO-regressed ensemble mean
North Pacific	1	28 ± 2.4	46.9 ± 9.8	31.6 ± 6.6
	2	19.7 ± 1.6	19.9 ± 4.1	19.9 ± 4.1
	3	12.7 ± 1.0	7.7 ± 1.6	12 ± 2.5
	4	7.4 ± 0.6	6.5 ± 1.3	8.7 ± 1.8
North Atlantic	1	37.5 ± 3.2	40 ± 8.4	37 ± 7.8
	2	21 ± 1.8	21.4 ± 4.5	26 ± 5.4
	3	12 ± 1.0	12.5 ± 2.6	12 ± 2.5
	4	10 ± 0.8	8.6 ± 1.8	7.5 ± 1.5

1) NORTH PACIFIC SECTOR

As in Fig. 3, Fig. 5 shows the first two modes of variability of the ensemble mean heights over the North Pacific. The PNA teleconnection pattern emerges as the

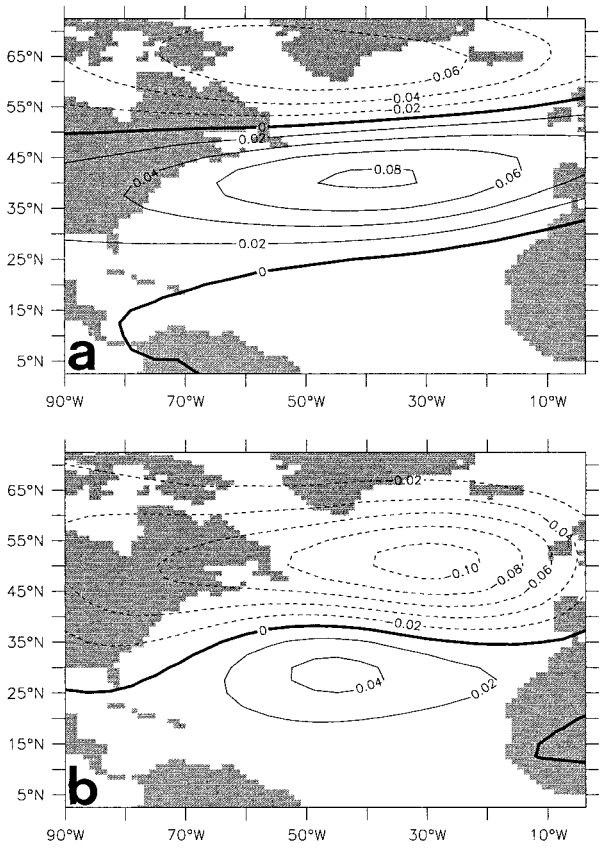

FIG. 4. As in Fig. 3 but for the North Atlantic modes of variability.

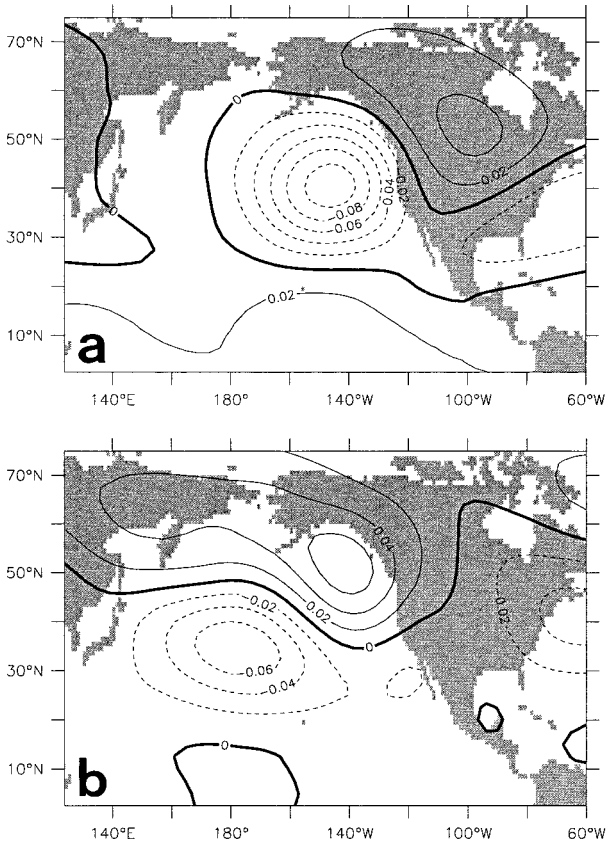

FIG. 5. As in Fig. 3 but for the ensemble mean winter geopotential height.

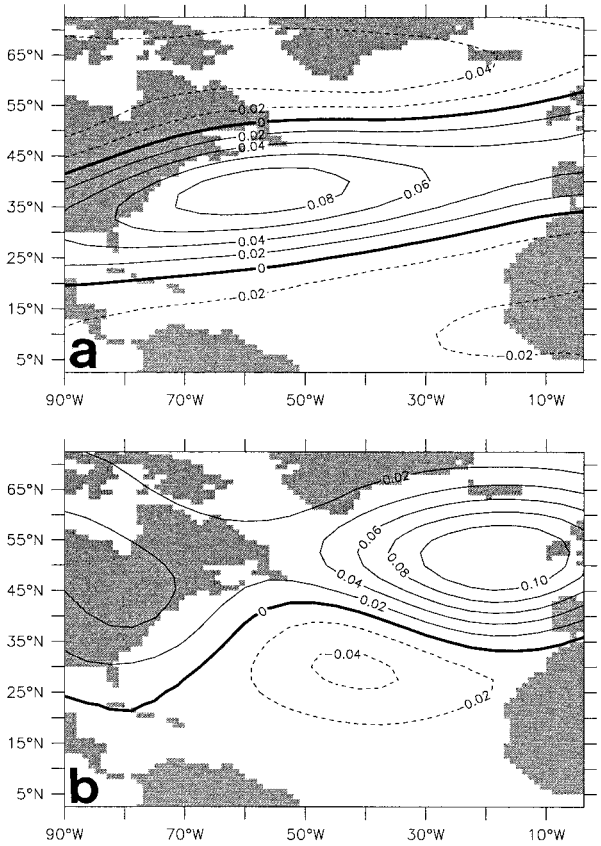

FIG. 6. As in Fig. 5 but for the North Atlantic sector.

leading mode with around 47% (Table 1) of the interannual variability while the second EOF shows a west and central-north Pacific mode similar to the first mode of the noise field, NPO, and explains around 20% of the total variability. The third mode with 8% variance (not shown) has a zonally oriented structure with a stronger center in the western part of the basin and is reminiscent of the West Pacific pattern.

2) NORTH ATLANTIC SECTOR

The first two modes of variability of the ensemble mean (Fig. 6) explain altogether around 61% of the total interannual variability and the first three explain as much variance as for the Pacific case (Table 1). Incidentally, Fig. 6, which can be compared to Fig. 4 with comparable explained variances indicates that, unlike the North Pacific case, the leading internal variability modes match those of the ensemble mean, that is, with the same ordering. This brings forward the question as to whether the ENSO has influence over the North Atlantic, which is discussed below.

The EOFs of the ensemble mean with the ENSO signal removed have also been computed. The leading modes (not shown) are found to be quite similar to the noise EOFs with similar explained variances (Table 1), see also the discussion below. Also computed are the Northern Hemisphere (NH) EOFs (not shown). The first NH mode of the noise indicates a polar–midlatitudes seesaw reminiscent of the Arctic oscillation (Thompson and Wallace 1998), accompanied by simultaneous weakening or strengthening of both Pacific and Atlantic jets. The second EOF shows a zonal wave with NPO signature and the third one shows the PNA pattern. The hemispheric EOF analysis of the ensemble mean indicates that the PNA, with 36% explained variance, emerges as the first mode with a downstream extension of the corresponding center over southeastern United States reaching as far as 50°E. The second mode, with 17% variance, is similar to the first NH internal mode.

c. Discussion

The EOF analysis over the North Pacific shows that the NPO comes first while the PNA comes second in the internal modes of variability. On the other hand, the PNA becomes first mode in the ensemble mean EOFs. Clearly this internal mode becomes locked to the east tropical Pacific SST anomalies since when the effect of ENSO was removed by regression the pattern ceases to be leading. This is in agreement with the observations made by Saravanan (1998) on the preference of partic-

ular modes, such as the PNA, in the presence of a SST variability. The locking to the tropical Pacific SST anomaly makes the PNA a ''long-lived'' pattern. It is noted in fact that this internal mode, which efficiently extracts energy from the mean state (Simmons et al. 1983; Blackmon et al. 1983), is observed on a wide range of timescales from days to months through seasons to decades (RRF98; Blackmon et al. 1983). The (linear) EOF analysis indicates unambiguously that most of the extratropical signal of ENSO projects onto the internal PNA mode.

Over the North Atlantic sector, on the other hand, the leading modes of the ensemble mean are basically undistinguishable from the corresponding internal modes. This point can also be noted in V99 where their SLP response to decadal changes in SST, with and without ENSO effect removed, is not too different from the leading EOF of the ensemble mean. Hence one is faced with two alternatives, namely; (i) there may be no response to ENSO over the North Atlantic or that the response is very weak and undistinguishable from the noise or (ii) the effect is nonlinear and therefore cannot be identified using for example linear techniques such as simple EOFs.

Now analyses performed by Lau and Nath (1994), for example, indicate that much of the atmospheric response to SST changes in the Global Ocean–Global Atmosphere experiment (GOGA) may be attributed to forcing in the tropical Pacific only, which is referred to as the Tropical Ocean Global Atmosphere experiment (TOGA) and that midlatitude SST anomalies are relatively inefficient in forcing the atmosphere (e.g., Palmer and Sun 1985; Kushnir and Held 1996). It is even argued that the observed SST changes in the extratropics are primarily responses to, rather than causes of, atmospheric changes (Trenberth and Hurrel 1994; Trenberth et al. 1998, hereafter T98 and references therein). A number of studies have in fact revealed a close connection between ENSO events and variability of remote oceans, such as the Atlantic, which is made possible through the ''atmospheric bridge'' mechanism (Lau and Nath 1996; Klein et al. 1999 and references therein). On the other hand, investigations carried out by Hoskins and Ambrizzi (1993) and others indicate that the atmospheric response to tropical forcing propagates downstream along well-defined waveguides. Hoskins and Karoly (1981) showed that the atmospheric response to tropical or subtropical heating propagates northward and eastward with a maximum at around 110° downstream of the forcing source. Therefore wave trains triggered, for example, by El Niño extend well into the Atlantic as pointed out by T98. Rossby waves generated by tropical Pacific SST forcing that propagate northeastward and then equatorward get reflected upon encountering a (sub)tropical easterly (Killworth and McIntyre 1985) and therefore can provide additional contributions to the atmospheric response over the North Atlantic.

Furthermore, in midlatitudes the SST response to the atmospheric driving patterns can in turn feed back onto the atmosphere (Trenberth and Hurrell 1994) inducing, therefore, nonlinearities in the forcing–response relationship. All the previous observations plus the relationship between internal and forced variabilities make up our conceptual framework of the nonlinear atmospheric response to ENSO over the North Atlantic sector, that is, point (ii) above. Now, even over the North Pacific the response is likely to be nonlinear since observational evidence indicates that there are in fact occasions where the PNA was not observed during some, although strong, El Niño events (T98). This nonlinear response is addressed next.

3. A probabilistic approach to signal detection

a. Motivation and background

A usual way to diagnose the atmospheric response, from observations, to a specific forcing is to make an ensemble average over the cases corresponding approximately to that forcing. Such approach suffers, however, a major drawback due essentially to (i) sampling, given the shortage of the observational records; (ii) reproducibility, since any two El Niños, for example, are never identical; and finally (iii) nonlinearity (HKZ97). GCMs have relatively eased the task through the possibility of making an ensemble of integrations although, theoretically, an infinite ensemble size is required in order for the ensemble mean to represent the model response to a given forcing. In practice, however, a finite ensemble of several integrations can be used to diagnose the response but the latter will always be noise contaminated as long as a proper filtering has not been applied.

The filtering requirement is particularly interesting since we now have an estimate of the noise. A natural way to deal with the problem is to look for patterns in state space that maximize the S:N ratio:

$$\max\rho = \frac{\mathbf{u}^{\mathrm{T}}\mathbf{C}_D\mathbf{u}}{\mathbf{u}^{\mathrm{T}}\mathbf{C}_N\mathbf{u}}, \tag{1}$$

where $\mathbf{C}_D$ is the covariance matrix of the sample data embedding the signal (the ensemble mean in this case) and $\mathbf{C}_N$ is the estimated noise (internal variability) covariance. Solutions to (1) can be obtained, for example, by solving a generalized eigenvalue problem:

$$\mathbf{C}_D\mathbf{u} = \rho\mathbf{C}_N\mathbf{u}. \tag{2}$$

Allen and Smith (1997, hereafter AS97) used a prewhitening operation to solve (1), and the vectors $\mathbf{u} = \mathbf{C}_N^{-1/2}\xi$, where ξ are the eigenvectors of the symmetric matrix $\mathbf{C}_N^{-1/2^{\mathrm{T}}}\mathbf{C}_D\mathbf{C}_N^{-1/2}$ with the largest eigenvalues, provide an optimal set of S:N maximizing patterns, optimal filters, known also as fingerprints (Hasselmann 1993; Thacker 1996). This approach has been applied by V99 to study the North Atlantic SLP response to varying SST (see the appendix for a brief description). The ap-

proach is an optimal technique particularly for Gaussian systems. However when the system departs from normality, as for the ENSO, for example (Burgers and Stephenson 1999), the approach can fail to identify a genuine signal (Hannachi 2000; and also Hannachi and Allen 2001). An alternative probabilistic approach (Hannachi 2000) that complements the S:N ratio approach would then be appropriate. It is formulated via the probability distribution functions (PDF) of the noise and the data. Next section, which presents a brief description of the method, provides a natural interpretation of the response and the S:N patterns, respectively. Theoretical details on the method can be found in Hannachi (2000).

b. A PDF approach to signal identification

In brief, the approach is based on the knowledge of the data and the noise PDFs, p_D and p_N, respectively. In the simple Gaussian case with

$$p_D(\mathbf{v}) = (2\pi)^{-m/2}|\mathbf{C}_D|^{-1/2}\exp\left[-\frac{1}{2}\mathbf{v}^{\mathrm{T}}\mathbf{C}_D^{-1}\mathbf{v}\right], \quad \text{and}$$

$$p_N(\mathbf{v}) = (2\pi)^{-m/2}|\mathbf{C}_N|^{-1/2}\exp\left[-\frac{1}{2}\mathbf{v}^{\mathrm{T}}\mathbf{C}_N^{-1}\mathbf{v}\right], \tag{3}$$

the signal orientation is sought in regions where p_N is at a minimum since the signal is expected to be easily captured in those regions. Now because we do not know the whereabouts of the signal contained in the data within the state space, equiprobable subsets of the data, that is, satisfying $\mathbf{v}^{\mathrm{T}}\mathbf{C}_D^{-1}\mathbf{v} = \alpha$ (α is a constant), are chosen over which p_N is minimized. This leads to

$$\max\ \mathbf{v}^{\mathrm{T}}\mathbf{C}_N^{-1}\mathbf{v} - \lambda(\mathbf{v}^{\mathrm{T}}\mathbf{C}_D^{-1}\mathbf{v} - \alpha), \tag{4}$$

or equivalently,

$$\mathbf{C}_D\mathbf{C}_N^{-1}\mathbf{v} = \lambda\mathbf{v}. \tag{5}$$

In (5) λ is a Lagrange multiplier. Therefore the response pattern comes out as the eigenvector corresponding to the leading eigenvalue of the *detection* matrix $\mathbf{C}_D\mathbf{C}_N^{-1}$ (Hannachi 2000). Now comparing (2) and (5) the optimal filter $\mathbf{u}$ (2) is simply the adjoint of the response pattern $\mathbf{v}$ and that $\mathbf{v} = \mathbf{C}_N\mathbf{u}$. Furthermore, in addition to being a S:N ratio an eigenvalue λ of the detection matrix $\mathbf{C}_D\mathbf{C}_N^{-1}$ is such that $\exp(-\lambda/2)$ represents the noise probability around the corresponding pattern within a unit element of volume of the state space. For example, in Hannachi (2000) the approach has been nicely illustrated with the Lorenz (1963) model.

The importance behind the PDF interpretation is the possibility to be extended to non-Gaussian cases. This is made possible via the fact that any PDF can be approximated as closely as desired by a finite mixture of Gaussians (Anderson and Moore 1979). For instance, p_D can be decomposed as

$$p_D(\mathbf{x}) = (2\pi)^{-m/2}\sum_{i=1}^{K}\alpha_i|\mathbf{C}_{D_i}|^{-1/2} \times \exp\left[-\frac{1}{2}(\mathbf{x} - \boldsymbol{\mu}_i)^{\mathrm{T}}\mathbf{C}_{D_i}^{-1}(\mathbf{x} - \boldsymbol{\mu}_i)\right], \tag{6}$$

where μ_i, $\mathbf{C}_{D_i}$, and α_i are, respectively, the center, the covariance matrix, and the proportion of the ith Gaussian forming the data with $\sum_{i=1}^{K}\alpha_i = 1$, and K is the total number of Gaussians. Now it can be shown (Hannachi 2000) that the problem of detecting the signal becomes equivalent to (5) over each Gaussian component, hence the signal pattern for the ith component corresponds simply to the leading eigenvector of

$$\mathbf{C}_{D_i}\mathbf{C}_N^{-1}\mathbf{v} = \lambda\mathbf{v}. \tag{7}$$

This theory fits quite nicely with atmospheric low-frequency variability (ALFV). In fact, there is an increasing trend among the climate community who thinks that the climate system is not a mere red noise of day-to-day fluctuations, but can display rather some sort of intermittent behavior between nonlinear circulation regimes (Palmer 1999; Corti et al. 1999). As pointed out by Palmer (1999), flow regimes have been found explicitly in both intermediate models and GCMs. There is also evidence that sectorial regimes exist such as teleconnection patterns (Wallace and Gutzler 1981). This behavior leads eventually to a significant departure from normality where the mixture model (6) (Everitt and Hand 1981) becomes a reasonable approximation to the ALFV and where the Gaussian components approximate the flow regimes (Haines and Hannachi 1995; Hannachi 1997). The PDF of the ensemble mean heights within the first two principal components (PCs) has been computed and shows signature of bimodality with respective centers $\pm$PNA (not shown) similar to those obtained by simple composite according to the ENSO phase (see section 4b).

4. Application to the atmospheric response

a. Quasi linearity and the atmospheric response over the North Pacific

Based on quasi linearity and prior to splitting the ensemble mean data, we analyze here the atmospheric response to ENSO over the North Pacific using the Gaussian approach [(2), (5)]. The results of this analysis enable us to compare them to those of section 4b and can therefore provide a better understanding of what is going on.

We display in Fig. 7 the adjoint mode $\mathbf{u}$ (Fig. 7a) and the response pattern $\mathbf{v}$, dual of $\mathbf{u}$, (Fig. 7b) of the geopotential height over the North Pacific sector. The response pattern (Fig. 7b) indicates a clear PNA. In Fig. 8 we display the time series of the projection of the ensemble mean and each of the ensemble members onto the adjoint mode. Note in particular the similarity be-

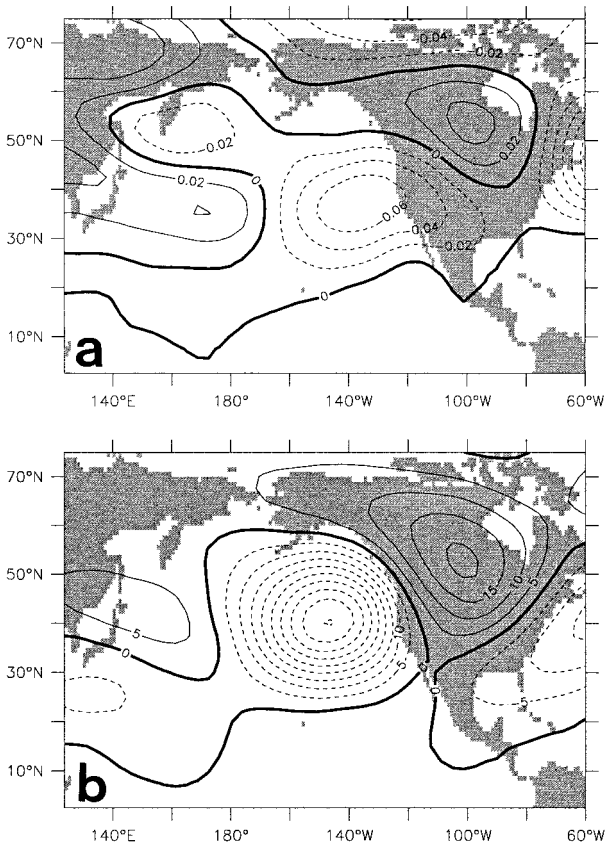

FIG. 7. (a) The adjoint mode and (b) the response pattern of the winter geopotential height over the North Pacific. Contour interval arbitrary in (a) and 5 m in (b).

tween these projections. The projection of the ensemble mean, which can be compared with Fig. 2, indicates that it is quite identical to the ENSO index with a correlation of order 0.90.

This (Gaussian) analysis clearly indicates the PNA mode as a linear response to ENSO that gets ''synchronized'' to it and with phase and amplitude, respectively, proportional to that of ENSO. Now there are several reasons to believe that this is not so in reality. In fact, asymmetries in the atmospheric response are obtained even when GCMs are forced by tropical SST anomalies, associated with El Niño and La Niña, that undergo identical evolution but with opposite phases (HKZ97). The previous response cannot explain the relationship between the nonlinear nature associated with the thermodynamic control on deep convection over the tropical Pacific and the teleconnection response over the northern midlatitudes (HKZ97). Also, the effect of opposite phases of (extreme) ENSO on atmospheric response tend to be asymmetrical [there is a saturation on the negative phase, Hoerling et al. (2001)]. Moreover, it is well documented that there are events of strong El Niño where the PNA, for example, is not observed (T98 and references therein).

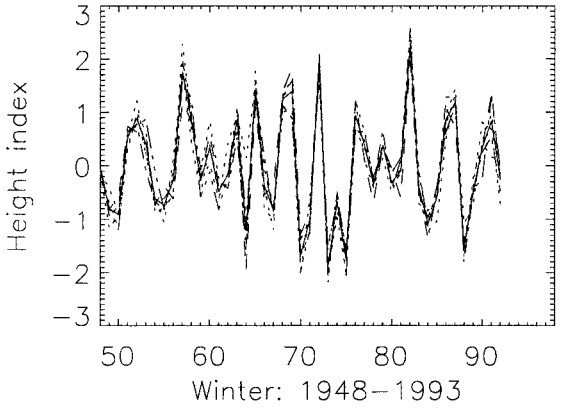

FIG. 8. The (standardized) time series obtained by projecting the winter geopotential heights of each ensemble member and the ensemble mean onto the corresponding adjoint mode (Fig. 7a).

b. Application of the nonlinear approach

First we compute significance between both ENSO phases events in the model. Figure 9 shows the difference between composite (DJF) 500-mb height anomalies corresponding to positive and negative phases over the North Pacific and Atlantic sectors, respectively, along with the 95% confidence level based on the *t*

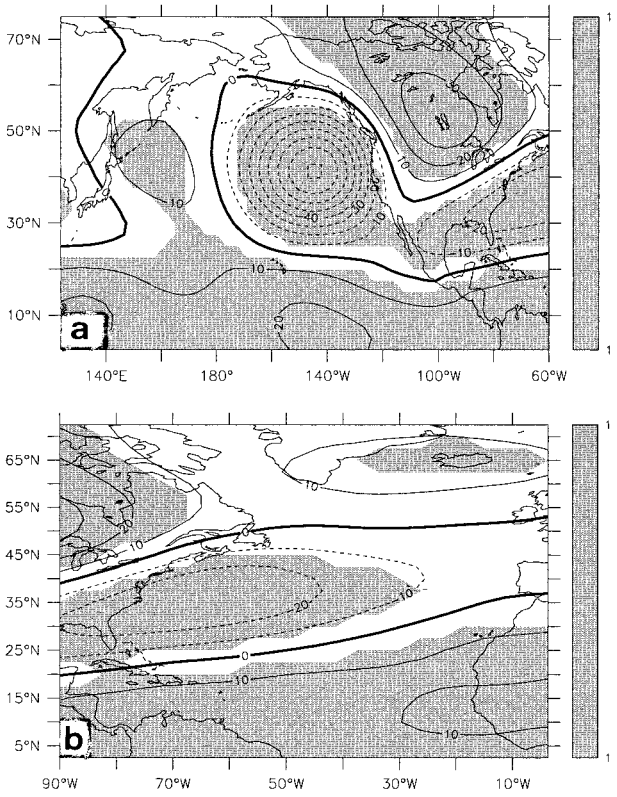

FIG. 9. Difference between composite DJF 500-mb height during positive and negative phases of ENSO over (a) the North Pacific and (b) North Atlantic. Positive contours are solid and negative contours are dashed. Contour interval 10 m.

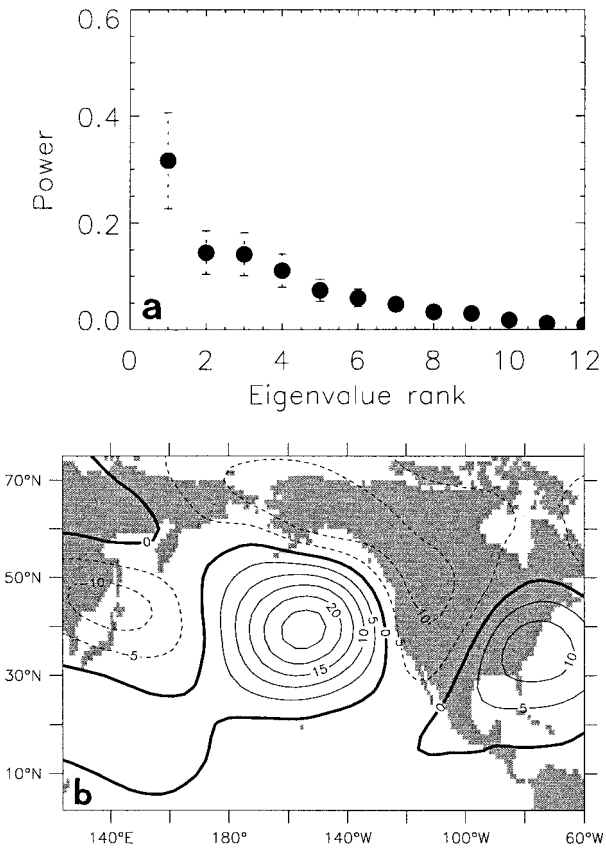

FIG. 10. (a) The spectrum of the detection matrix during La Niña and (b) the response pattern corresponding to the leading eigenvalue. Contour interval is 5 m in (b).

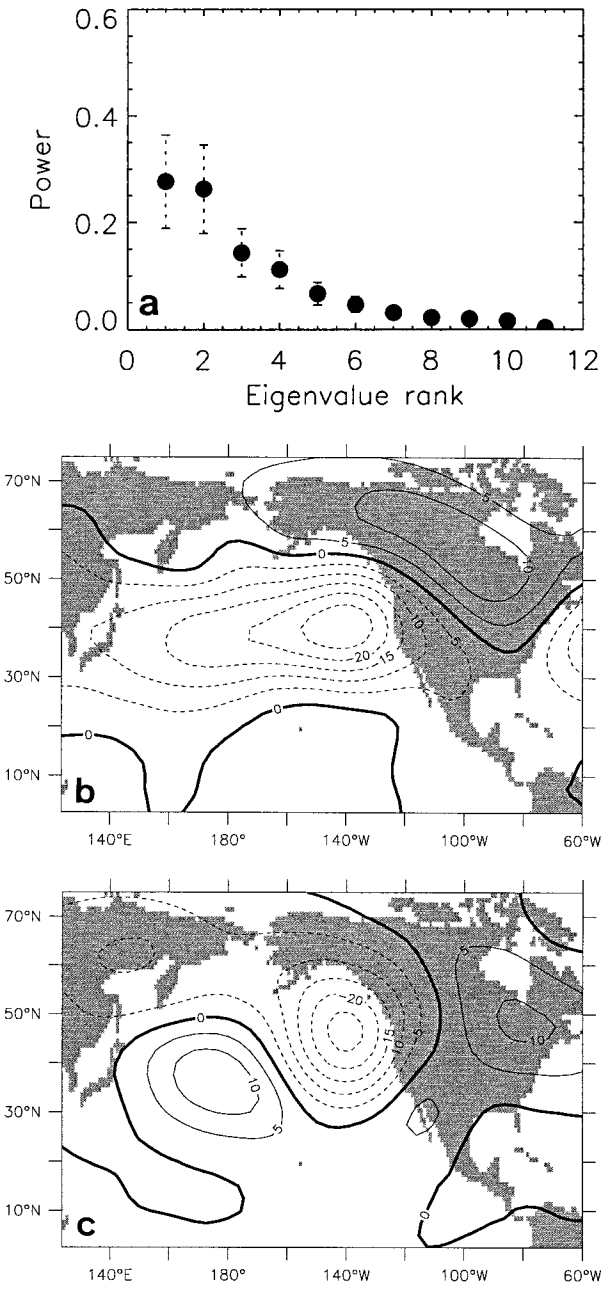

FIG. 11. (a) The spectrum of the detection matrix during El Niño and (b), (c) the response patterns corresponding to the leading two degenerate eigenvalues. Contour interval 5 m.

statistic with serial correlation (Kendall and Ord 1990) taken into account. Note in particular the significance of most centers over both sectors.

Now to apply the theory presented in section 3b the data are classified into regimes given that these data support a non-Gaussian behavior with two regimes over both basins. For convenience we simply classify the data according to the sign of the Niño-3 index and then apply the approach to each subset separately. In this way the results can be easily interpreted and also compared to other studies.

Figure 10a displays the spectrum of the detection matrix during La Niña showing a leading nondegenerate eigenvalue that corresponds to a negative PNA (Fig. 10b). The spectrum during El Niño (Fig. 11a) indicates, however, a degenerate leading eigenvalue with therefore more than one response (Fig. 11). The first pattern (Fig. 11b) shows a zonally stretched PNA-like mode and incorporates some features from the NPO-like pattern (Figs. 3a and 5b) especially over the open ocean. The low center (Fig. 11b) is zonally stretched with its minimum (40°N, 140°W) being closer to the continent than the corresponding center of Fig. 10b (40°N, 155°W). The second pattern (Fig. 11c) indicates a slightly zonal structure with main centers located, respectively, over the western part of the basin, the Gulf of Alaska, and Eastern Canada and bears some similarities to the tropical Northern Hemisphere (T98).

Note particularly that none of the responses during El Niño are the reverse of that during La Niña and that the correlation between the patterns of Figs. 10b and 11b is 0.40 and only 0.10 between Figs. 10b and 11c. It is possible that these two circulation responses (Fig. 11) are associated with different tropical forcings that

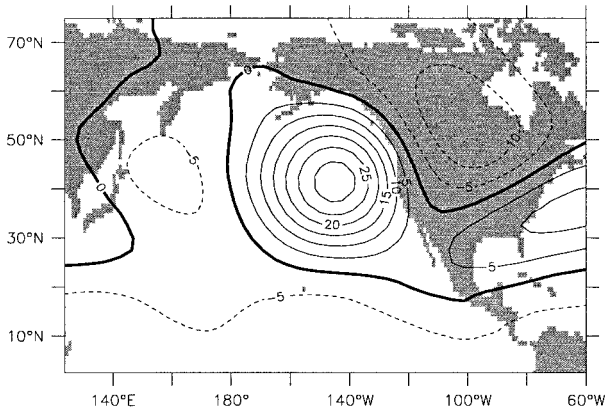

FIG. 12. Composite of the geopotential height anomalies during cold events. Contour interval 5 m.

trigger them and one needs a longer time series in order to properly address this question.

To compare the previous patterns to those obtained by simple composite, Fig. 12 shows the composite height anomalies during cold events. The warm composite (not shown) is the reverse of Fig. 12 (see also Fig. 9a). Note that results from the nonlinear analysis are in agreement with the fact that flows other than the PNA pattern can be observed during ENSO events (T98). The rms of the response during La Niña is 7.2 m while it is 8.2 and 6.6 m for the first and second pattern responses during El Niño. Note particularly the small difference between the rms of the linear response, 9.8 m, and that of the nonlinear response during El Niño.

On the basis of this nonlinearity one might argue that, given the (nonlinear) asymmetries in the Niño-3 index between both phases, nonlinearity in SST already precedes the atmospheric response. Precisely, prior to the midlatitude atmospheric response, nonlinearity has already manifested, for example, in the tropical rainfall. The truth is that this can happen even when GCMs are forced by tropical SST anomalies, associated with El Niño and La Niña, that undergo identical evolution but with opposite phases (HKZ97). Furthermore, simple composite analysis of the 500-mb heights corresponding to extreme warm and cold events of the tropical Pacific performed by HKZ97, reveals planetary teleconnection patterns with an appreciable phase shift between the warm and cold event circulation composite anomalies.

Now since the analysis based on quasi-linearity indicates an overall PNA pattern (Fig. 7b) whose phase (and also amplitude) changes with the phase (and amplitude) of the SST anomaly corresponding to El Niño and La Niña (Figs. 2 and 8), the connection to the present nonlinear analysis shows that the quasi-linear response pattern is much similar to the response corresponding to La Niña (cf. Figs. 7b and 10b). The point is that the diagnostic of the atmospheric response to changes in the tropical Pacific SST based on linearity (section 4a) is more likely to be biased, that is dominated by the response to one of the forcing modes, here La Niña that appears to shadow the response to El Niño, indicating therefore the importance of the nonlinear approach.

Zonal asymmetries of the climatological SSTs can be very important in shaping asymmetries between the effects of El Niño and La Niña. As pointed out by Holton (1992), tropical anomalies have their greatest effect in the western Pacific where even a small SST anomaly can excite large rainfall deviation on the periphery of the west Pacific warm pool region whereas positive anomalies of appreciable amplitude are required to induce convection in the east equatorial Pacific (HKZ97). As for the shadowing effect it may be, as indicated by Webster and Chang (1981) that because the perturbation kinetic energy ($\overline{PKE}$; Webster and Chang 1981) is large over the tropical Pacific, very strong westerlies (westerly ducts) occur in the upper troposphere, allowing for tropical–extratropical exchange, whereas during El Niño westerlies are weaker than in the La Niña phase.

Because of the complicated nature of the atmospheric variability over the North Atlantic due to several factors including local effects and large internal dynamics, there was a lack of interest in the ENSO effect on the basin. The previous factors can in fact contribute to the nonlinear response that is addressed next. As for the Pacific case the data are first split according to the ENSO phase. The EOF analysis indicates that the first mode during El Niño and the same one during La Niña (not shown) look, respectively, like Figs. 6b and 6a implying, therefore, further support on the influence of ENSO.

The analysis of the spectrum of the detection matrix shows, like the Pacific case, that during La Niña the response is nondegenerate while it is degenerate during El Niño. Figure 13 shows the first response pattern during El Niño (Fig. 13a) and the pattern during La Niña (Fig. 13b). The second pattern corresponding to El Niño (not shown) indicates two major centers over south of Iceland and Newfoundland, respectively, and a minor center over the southeast of the United States. Note the similarity between Figs. 13a, 13b, and Figs. 4b, 4a (and also 6b, 6a) indicating that the response patterns during warm and cold events, respectively, are not very far from quadrature. In fact, the correlation between the patterns of Fig. 13 is only 0.30. Note also that the rms corresponding to Figs. 13a and 13b are, respectively, 5.94 and 5.48 m compared to 6.1 m for the linear response. As in Fig. 12, we display in Fig. 14 the composite of height anomalies during La Niña. The composite during the opposite phase (not shown) is the reverse of Fig. 14.

During warm events the first response has a tilted northeast–southwest dipole structure with respective centers located over northeast and the western middle North Atlantic (Fig. 13a). This pattern projects quite reasonably onto the NAO with a north–south seesaw that modulates the strengthening and the weakening of the North Atlantic jet. Note in particular the out-of-

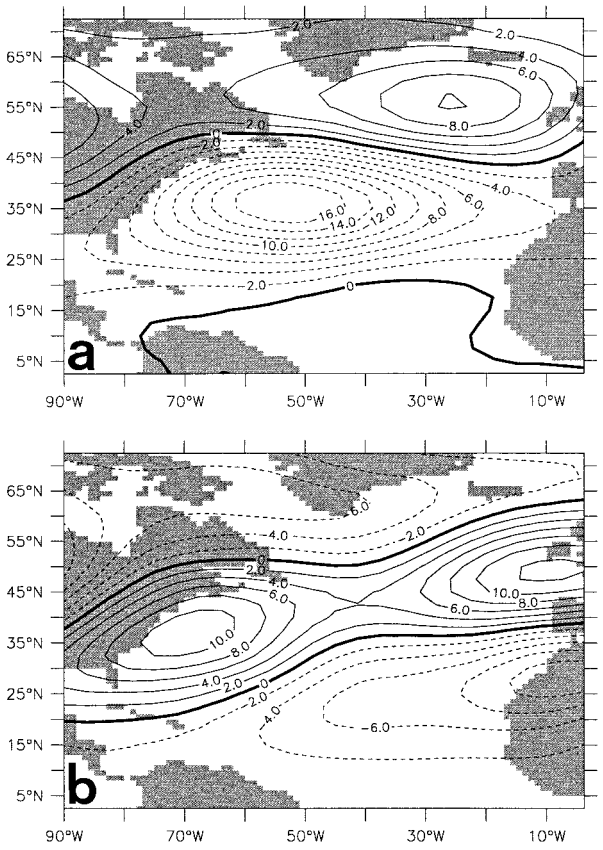

FIG. 13. (a) The first response pattern of the winter geopotential height over the North Atlantic during El Niño and (b) the response during La Niña. Contour interval 2 m.

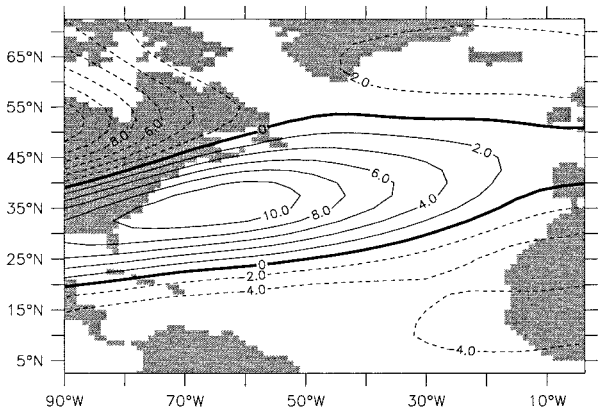

FIG. 14. As in Fig. 12 but for the North Atlantic. Contour interval 2 m.

phase anomalous pattern between Iceland and the Azores a main feature of NAO (Hurrell 1995).

On the other hand, during cold events the atmospheric response over the North Atlantic sector has a kind of tripole structure (Fig. 13b). Note, unlike Fig. 13a, the in-phase anomalous pattern between Iceland and the Azores, which is due to the existence of the southern anomalous center over western North Africa that stretches westward into the eastern and central North Atlantic. In a typical NAO this center is usually shifted southward. This response corresponds essentially to a northward and southward shift of the subtropical and Icelandic high pressure systems, respectively.

Although the internal noise over the North Atlantic sector is larger than the corresponding one over the North Pacific, the signals obtained over the former sector are still optimally filtered. However, it can be noted that the western North Atlantic part of the signal is somewhat related to the signal obtained over the PNA region. As for the eastern part of the signal one does not rule out the influence of the (small) sample size, for example, and it would certainly be of great benefit to extend this analysis to a longer time series with a larger sample of the ensemble.

The comparison of Figs. 11b,c to the observed warm composite (HKZ97) shows that the observed features are reasonably well represented. For instance the high pressure over North America is well represented in Fig. 11b while the remaining structure over the ocean is well represented in Fig. 11c. The main features of the observed cold composite over the North Atlantic also are reasonably well captured by Fig. 13b.

Investigations of the extratropical response to a heating anomaly in the central Pacific using barotropic dynamics performed by Branstator (1985) indicates a typical similarity of the response over the North Atlantic to Fig. 13a (see also Fig. 9b of T98) and also of the response over the North Pacific to Fig. 11b. In general, however, and owing to discrepancies between different models (HKZ97; Gershunov and Barnett 1998) one cannot exclude the possible dependence of the results to the particular GCM employed. For instance comparing Fig. 13 against the National Centers for Environmental Prediction climate model's composite warm and cold event signals (HKZ97) reveals appreciable differences over the North Atlantic. Even over the North Pacific, models may still disagree as is shown in the one-sided linear regression in the ECHAM and the Geophysical Fluid Dynamics Laboratory models respectively (Hoerling et al. 2001).

5. Summary and conclusions

We analyzed in this manuscript a set of multidecadal GCM runs in order to study the atmospheric response to ENSO. The analysis used a set of six independent model integrations of 45 years each from the Hadley Centre GCM model, HadAM1, forced by observed SST and focused on the winter 500-mb heights over the North Pacific and North Atlantic sectors. The model noise is estimated as the departure of the ensemble members from the ensemble mean. The familiar PNA pattern emerges as second mode of internal variability while the first mode is reminiscent of the NPO over the North Pacific. For the ensemble mean, the same PNA mode

appears as first mode of variability over the North Pacific while over the North Atlantic the first modes of variability are not too different from the corresponding modes of the internal noise.

The EOF analysis indicates that the PNA behaves as a (quasi-linearly) locked mode to the ENSO while over the North Atlantic the atmospheric response is more likely nonlinear. To optimally filter the signal out, this latter is defined as the pattern maximizing the ensemble mean PDF on isopleths of the noise (internal variability) PDF, leading to the eigenvector corresponding to the leading eigenvalue of the detection matrix $\mathbf{C}_D\mathbf{C}_N^{-1}$. When the data present a non-Gaussian behavior, the same approach is applied to each Gaussian component forming the data.

The Gaussian analysis applied to the North Pacific sector indicates the PNA pattern as a synchronized response to ENSO with +PNA during El Niño and −PNA during La Niña and the amplitude of the response being proportional to the amplitude of the east tropical Pacific SST anomaly. This response, however, seems inconsistent with the nonlinear nature involved in the relationship between the SST forcing and the atmospheric response (HKZ97). It is also well documented that there are events of strong ENSO without the PNA being observed (T98).

In order to find the nonlinear signal, the ensemble mean data is split into regimes according to the sign of the Niño-3 index (for simplicity and convenience) and then the signal over each cluster obtained. This choice was supported by the non-Gaussian behavior of the data over both basins.

Over the North Pacific, La Niña triggers the −PNA pattern whereas during El Niño the response is degenerate with more than one pattern solution. The first pattern appears as a zonally stretched PNA that bears some feature of NPO and with the Pacific center closer to the continent than the corresponding center of the previous pattern. The second pattern is similar to the tropical Northern Hemisphere mode (T98). None of these two patterns is precisely the reverse of −PNA.

Over the North Atlantic the analysis also indicates that the response during El Niño is degenerate and that the patterns corresponding to La Niña and El Niño have weak correlations. The first atmospheric response to El Niño shows a north–south dipole tilted northeast–southwest bearing some similarities, but not identical, to the NAO while during La Niña, a tripole structure emerges.

The pattern responses show that the observed features are reasonably well captured. They also agree well with results obtained by Branstator (1985) using barotropic dynamics. Finally, although this study is based on HadAM1 and owing to possible discrepancies between different models, it is not impossible that the results can be model dependent, and it would be of great benefit to compare the results of the current analysis with different models such as those submitted to the Atmospheric Model Intercomparison Project run.

Acknowledgments. The Hadley Centre is acknowledged for providing the HadAM1 simulations. Particular thanks go to S. Brown for his help in getting the HadAM1 data and D. Rowell for his comments on the text. Discussions with M. R. Allen and R. Sutton are very much appreciated. I am also grateful to G. Branstator for stimulating discussions and comments on the paper and also for hosting me during a visist to NCAR and would like to thank two anonynmous reviewers for their constructive reviews that improved the manuscript. This work was supported by U.K. Universities Global Atmospheric Modelling Project (UGAMP).

APPENDIX

The Spectrum of the Detection Matrix

This is a brief outline of the use of singular value decomposition (SVD) to obtain the spectrum of the detection matrix $\mathbf{C}_D\mathbf{C}_N^{-1}$ and the response patterns [Eqs. (2) and (5)]. Given the noise and the ensemble mean fields $\mathbf{X}_N$ and $\mathbf{X}_D$, respectively, and adopting the notation $\mathbf{C}_{N,D} = \mathbf{X}_{N,D}\mathbf{X}_{N,D}^{\mathrm{T}}$, a SVD is first applied to $\mathbf{X}_N$:

$$\mathbf{X}_N = \mathbf{E}_N\mathbf{\Lambda}_N\mathbf{P}_N^{\mathrm{T}} \tag{A1}$$

leading to the EOFs, $\mathbf{E}_N$, and singular values, $\mathbf{\Lambda}_N$ of the noise. To mimic the eigenspectrum of the symmetric matrix $\mathbf{C}_N^{-1/2^{\mathrm{T}}}\mathbf{C}_D\mathbf{C}_N^{-1/2}$, a weighted projection, $\boldsymbol{\chi}_D$, of the ensemble mean onto the noise EOFs is first performed and a SVD is then applied:

$$\boldsymbol{\chi}_D = \mathbf{\Lambda}_N^{-1}\mathbf{E}_N^{\mathrm{T}}\mathbf{X}_D = \mathbf{E}'\mathbf{\Lambda}'\mathbf{P}'^{\mathrm{T}}. \tag{A2}$$

Note that the spectrum of the detection matrix (S:N ratios) is given by $\mathbf{\Lambda}'^2$. Also to neglect the effect of high-order noise EOFs, a subset of the spectrum of the noise is used in practice when projecting the ensemble mean. The response patterns, $\mathbf{V}$, (5) and the adjoint modes, $\mathbf{U}$, (2) are then respectively given by

$$\mathbf{V} = \mathbf{C}_N^{1/2^{\mathrm{T}}}\mathbf{E}' = \mathbf{E}_N\mathbf{\Lambda}_N\mathbf{E}', \tag{A3}$$

$$\mathbf{U} = \mathbf{C}_N^{-1}\mathbf{V} = \mathbf{E}_N\mathbf{\Lambda}_N^{-1}\mathbf{E}'. \tag{A4}$$

REFERENCES

Allen, M. R., and L. A. Smith, 1997: Optimal filtering in singular spectrum analysis. *Phys. Lett. A,* **234,** 419–428.

Anderson, B. O., and J. B. Moore, 1979: *Optimal Filtering.* Prentice Hall, 357 pp.

Blackmon, M. L., J. E. Giesler, and E. J. Pitcher, 1983: A general circulation study of January climate anomaly patterns associated with interannual variation of equatorial Pacific SSTs. *J. Atmos. Sci.,* **40,** 1410–1425.

Branstator, G., 1985: Analysis of general circulation model sea-surface temperature anomaly simulations using a linear model. Part I: Forced solutions. *J. Atmos. Sci.,* **42,** 2225–2241.

Burgers, G., and D. B. Stephenson, 1999: The 'normality' of El Niño. *Geophys. Res. Lett.,* **26,** 1027–1030.

Corti, S., F. Molteni, and T. N. Palmer, 1999: Signature of recent climate change in frequencies of natural atmospheric circulation regimes. *Nature,* **398,** 799–802.

Davies, J. R., D. P. Rowell, and C. K. Folland, 1997: North Atlantic

and European seasonal predictability using an ensemble of multi-decadal AGCM simulations. *Int. J. Climatol.,* **17,** 1263–1284.
Everitt, B. S., and D. J. Hand, 1981: *Finite Mixture Distributions.* Chapmann and Hall, 143 pp.
Gershunov, A., and T. P. Barnett, 1998: ENSO influence on intra-seasonal extreme rainfall and temperature frequencies in the contiguous United States: Observations and model results. *J. Climate,* **11,** 1575–1586.
Haines, K., and A. Hannachi, 1995: Weather regimes in the Pacific from a GCM. *J. Atmos. Sci.,* **52,** 2444–2462.
Hannachi, A., 1997: Low-frequency variability in a GCM: Three-dimensional flow regimes and their dynamics. *J. Climate,* **10,** 1357–1379.
——, 2000: Probabilistic-based approach to optimal filtering. *Phys. Rev. E,* **61,** 3610–3619.
——, and M. R. Allen, 2001: Identifying signals from intermittent low-frequency behaving systems. *Tellus,* in press.
Hasselmann, K., 1993: Optimal fingerprints for the detection of time-dependent climate change. *J. Climate,* **6,** 1957–1969.
Hoerling, M. P., A. Kumar, and M. Zhong, 1997: El Niño, La Niña, and the nonlinearity of their teleconnections. *J. Climate,* **10,** 1769–1786.
——, ——, and T. Xu, 2001: Robustness of the nonlinear climate response to ENSO's extreme phases. *J. Climate,* **14,** 1277–1293.
Holton, J. R., 1992: *An Introduction to Dynamic Meteorology.* Academic Press, 511 pp.
Horel, J. D., and J. M. Wallace, 1981: Planetary-scale atmospheric phenomena associated with the Southern Oscillation. *Mon. Wea. Rev.,* **109,** 813–829.
Hoskins, B. J., and D. J. Karoly, 1981: The steady linear response of a spherical atmosphere to thermal and orographic forcing. *J. Atmos. Sci.,* **38,** 1179–1196.
——, and T. Ambrizzi, 1993: Rossby wave propagation on a realistic longitudinally varying flow. *J. Atmos. Sci.,* **50,** 1661–1671.
Hurrell, J. W., 1995: Decadal trends in the North Atlantic Oscillation: Regional temperatures and precipitation. *Science,* **269,** 676–679.
Kendall, M., and J. K. Ord, 1990: *Time Series.* Edward Arnold, 296 pp.
Killworth, P. D., and M. E. McIntyre, 1985: Do Rossby-wave critical layers absorb, reflect, or over-reflect. *J. Fluid Mech.,* **161,** 449–492.
Klein, S. A., B. S. Soden, and N.-C. Lau, 1999: Remote sea surface temperature variations during ENSO: Evidence for a tropical atmospheric bridge. *J. Climate,* **12,** 917–932.
Kushnir, Y., and I. M. Held, 1996: Equilibrium atmospheric response to North Atlantic SST anomalies. *J. Climate,* **9,** 1208–1220.
Lau, N.-C., and M. J. Nath, 1994: A modeling study of the relative roles of tropical and extratropical SST anomalies in the variability of the global atmosphere–ocean system. *J. Climate,* **7,** 1184–1207.
——, and ——, 1996: The role of the atmospheric bridge in linking tropical Pacific ENSO events to extratropical SST anomalies. *J. Climate,* **9,** 2036–2057.
Livezey, R. E., A. Leetmaa, M. Mautani, H. Rui, N. Ji, and A. Kumar, 1997: Teleconnective response of the Pacific–North American region atmosphere to large central equatorial Pacific SST anomalies. *J. Climate,* **10,** 1787–1820.
Lorenz, E. N., 1963: Deterministic nonperiodic flow. *J. Atmos. Sci.,* **20,** 130–141.
North, G. R., T. L. Bell, R. F. Cahalan, and F. G. Moeng, 1982: Sampling errors in the estimation of the empirical orthogonal functions. *Mon. Wea. Rev.,* **110,** 699–706.
Palmer, T. N., 1999: A nonlinear dynamical perspective on climate prediction. *J. Climate,* **12,** 575–591.
——, and Z. Sun, 1985: A modelling and observational study of the relationship between sea surface temperature in the north west Atlantic and the atmospheric general circulation. *Quart. J. Roy. Meteor. Soc.,* **111,** 947–975.
Parker, D. E., C. K. Folland, A. Bevan, M. N. Ward, M. Jackson, and F. Maskell, 1995: Marine surface data for analysis of climate fluctuations on interannual to century timescales. *Natural Climate Variability on Decadal to Century Timescales,* D. G. Martinson et al., Eds., National Academy Press, 241–250.
Phillips, T. J., 1994: A summary documentation of the AMIP models. PCMDI Rep. 18, University of California, 343 pp. [Available from Lawrence Livermore National Laboratory, University of California, Livermore, CA 94550.]
Renshaw, A. C., D. P. Rowell, and C. K. Folland, 1998: Wintertime low-frequency weather variability in the North Pacific–American sector 1949–93. *J. Climate,* **11,** 1073–1093.
Rowell, D. P., 1998: Assessing potential seasonal predictability with an ensemble of multidecadal GCM simulations. *J. Climate,* **11,** 109–120.
Saravanan, R., 1998: Atmospheric low-frequency variability and its relationship to midlatitude SST variability: Studies using the NCAR climate system model. *J. Climate,* **11,** 1386–1404.
Simmons, A. J., J. M. Wallace, and G. W. Branstator, 1983: Barotropic wave propagation and instability, and atmospheric teleconnection patterns. *J. Atmos. Sci.,* **40,** 1363–1392.
Thacker, W. C., 1996: Climatic fingerprints, patterns and indices. *J. Climate,* **9,** 2259–2261.
Thompson, D. W. J., and J. M. Wallace, 1998: The Arctic Oscillation signature in the wintertime geopotential height and temperature fields. *Geophys. Res. Lett.,* **25,** 1297–1300.
Trenberth, K. E., and J. W. Hurrell, 1994: Decadal atmospheric-ocean variations in the Pacific. *Climate Dyn.,* **9,** 303–309.
——, G. W. Branstator, D. Karoly, A. Kumar, N.-C. Lau, and C. Ropelewski, 1998: Progress during TOGA in understanding and modeling global teleconnections associated with tropical sea surface temperatures. *J. Geophys. Res.,* **103,** 14 291–14 324.
Venzke, S., M. R. Allen, R. T. Sutton, and D. P. Rowell, 1999: The atmospheric response over the North Atlantic to decadal changes in sea surface temperature. *J. Climate,* **12,** 2562–2584.
Wallace, J. M., and D. S. Gutzler, 1981: Teleconnections in the geopotential height field during the Northern Hemisphere winter. *Mon. Wea. Rev.,* **109,** 784–812.
Webster, P. J., and H.-R. Chang, 1988: Equatorial energy accumulation and emanation regions: Impacts of a zonally varying basic state. *J. Atmos. Sci.,* **45,** 803–829.